Bulk-boundary correspondence from the intercellular Zak phase

Jun-Won Rhim, Jan Behrends, and Jens H. Bardarson

Max-Planck-Institut für Physik komplexer Systeme, 01187 Dresden, Germany

The Zak phase γ, the generalization of the Berry phase to Bloch wave functions in solids, is often used to characterize inversion-symmetric one-dimensional (1D) topological insulators. Due to its dependence on the real-space origin and unit cell, however, there is an ambiguity in its use in a bulk-boundary correspondence. Here, we extract an origin-independent part of γ, the so-called intercellular Zak phase γ^{inter}, and show that it is a bulk quantity that unambiguously predicts the number of surface modes. Specifically, a neutral finite 1D tight-binding system has $n_s = \gamma^{\text{inter}}/\pi$ (mod 2) in-gap surface modes below the Fermi level if there exists a commensurate inversion-symmetric bulk unit cell. We demonstrate this in two steps: First, we verify that $\pm e\gamma^{\text{inter}}/2\pi$ (mod e) equals the extra charge accumulation in the surface region in a terminated system of a translationally invariant 1D insulator, while the remnant part of γ, the intracellular Zak phase γ^{intra}, corresponds to the electronic part of the bulk's unit-cell dipole moment. Second, we show that the extra charge accumulation is related to the number of surface modes when the unit cell is inversion symmetric. We study several tight-binding models to quantitatively check both the relation between the extra charge accumulation and the intercellular Zak phase, and the bulk-boundary correspondence using the intercellular Zak phase.

I. INTRODUCTION

The Berry phase is a geometric phase of eigenstates obtained when cyclically varying external parameters [1]. For a Hamiltonian $\mathcal{H}(\mathbf{R})$ that depends on the external parameters $\mathbf{R}$, the Berry phase is given by

$$\gamma_n = i \oint_C \langle n(\mathbf{R})|\nabla_{\mathbf{R}}|n(\mathbf{R})\rangle \cdot d\mathbf{R}, \tag{1}$$

where $|n(\mathbf{R})\rangle$ is the nth eigenvector and C is a closed loop in the parameter space of $\mathbf{R}$. In a Brillouin zone, as pointed out by Zak [2], a natural choice for the cyclic parameter is the crystal momentum k. The explicit form of the resulting Zak phase of the nth band is

$$\gamma_n = i \int_{\text{BZ}} dk \langle u_{n,k}|\partial_k|u_{n,k}\rangle, \tag{2}$$

where BZ represents the one-dimensional (1D) Brillouin zone, and $u_{n,k} = \sqrt{N}e^{-ikx}\psi_{n,k}$ is the periodic part of the Bloch function $\psi_{n,k}$. The total Zak phase γ is obtained by summing γ_n over filled bands.

The Zak phase was endowed with a physical meaning with the modern definition of the polarization $\mathbf{P}$, introduced by Vanderbilt and King-Smith [3,4]. The ambiguity of the classical polarization, which depends on the shape of the unit-cell boundary [5], was resolved by redefining the electronic part of the polarization $\mathbf{P}^{\text{el}}$ as an integral of Wannier functions over the whole space, rather than over a unit cell. With this definition, one can accurately predict the bound surface charge $\sigma = \mathbf{P} \cdot \hat{n}$, with $\hat{n}$ the surface orientation, measured in capacitance experiments [6]. Furthermore, the electronic polarization $P_{\perp}^{\text{el}}$ along $\hat{n}$ is related to the Zak phase (evaluated along $\hat{n}$ with $\mathbf{k}_{\parallel}$ kept fixed) via

$$P_{\perp}^{\text{el}} = \mathbf{P}^{\text{el}} \cdot \hat{n} = -\frac{e}{(2\pi)^3} \int_{\mathcal{A}} d\mathbf{k}_{\parallel} \sum_{n=1}^{Z} \gamma_n, \tag{3}$$

where $\mathcal{A}$ is the two-dimensional (2D) Brillouin zone projected to the 2D plane perpendicular to $\hat{n}$, $\mathbf{k}_{\parallel}$ is the momen-

tum component in this plane, and Z the number of filled bands.

In the currently active study of topological aspects of materials [7–15], the Zak phase has been utilized as a topological number to classify various genuine 1D topological insulators, as well as effective ones, such as those obtained by fixing one or two momenta of 2D or 3D Hamiltonians [16–34]; it was naturally extended to the concept of non-Abelian Wilson loops in the multiband case and used for classifications of topological insulators with inversion or nonsymmorphic symmetries and topological crystalline insulators [35–40]. Furthermore, the Zak phase has been widely used for the Z_2 classification of inversion-symmetric 1D systems where it is quantized to 0 or π (mod 2π) [2]. In this case, the conventional bulk-boundary correspondence states that there are boundary modes if the Zak phase is nontrivial, $\gamma = \pi$, while $\gamma = 0$ is considered a trivial insulator without surface modes [17–22].

Recent work, however, pointed out that the Zak phase depends on the gauge choice of choosing the origin of the real space, and how one defines boundaries of the unit cell, although it is invariant under gauge transformation of the form $u_{n,k} \to e^{i\phi_k}u_{n,k}$ [25,30,31]. This means that the Zak phase itself is not a well-defined topological number since it cannot characterize the bulk uniquely. In an attempt to resolve this ambiguity, Atala *et al.* [25] suggested that the difference of the Zak phase between different states could be a proper topological number, and Juan *et al.* [30] revised the Zak phase by adding a unit-cell-dependent term such that the resultant Z_2 number plays the role of a gauge-invariant topological number. In spite of these issues, the conventional bulk-boundary correspondence using the Zak phase has been successfully applied in many cases [17–22]. Furthermore, additional conditions for the applicability of the correspondence to finite systems have been given, such as that terminated edges should not break the inversion symmetry of the bulk [41,42] or that the finite system should be commensurate with the bulk's unit cell [30]. However, the necessity of those assumptions has not been demonstrated in general 1D systems, and we in fact find that
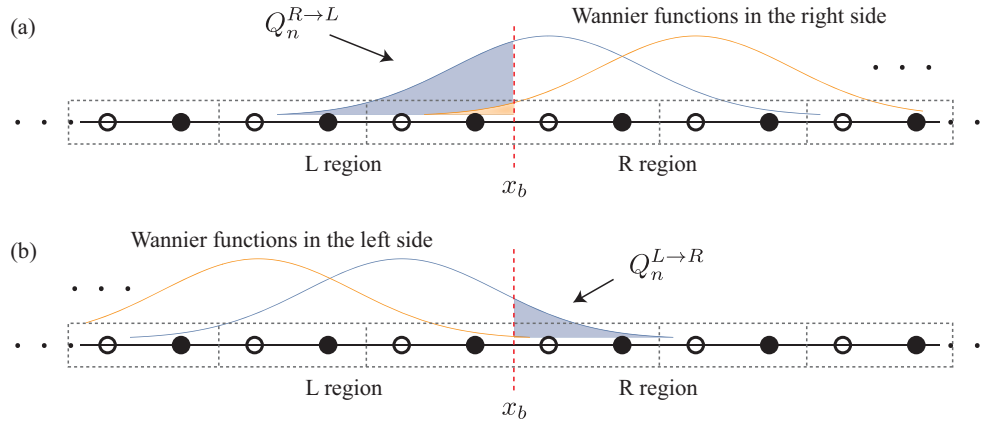
FIG. 1. A schematic figure describing a general 1D system and its Wannier functions. Gray dashed boxes are the unit cells, which contain atomic sites marked by filled and empty circles as an example. Each unit cell can in general have any number of atomic sites. The 1D bulk is divided into left and right sides with respect to a given unit-cell boundary x_b, which is marked by the red dashed line. We call these regions the L and R regions. Wannier functions belong to the left or right side according to their centers. $Q_n^{R \to L}$ represents how much weight of right side's Wannier functions are in the left side, and vice versa for $Q_n^{L \to R}$.

the conventional bulk-boundary correspondence using γ can fail even in the presence of inversion symmetry both in the bulk and terminated systems (cf. Sec. V B).

In this paper, we resolve these issues by providing a more detailed analysis of the Zak phase, dealing with general 1D tight-binding models. To this end, we split the Zak phase into two terms, the *intracellular* and *intercellular* Zak phase (this splitting was earlier introduced by Kudin *et al.* [43]), and provide them with their proper physical interpretations. The intracellular Zak phase γ^{intra} describes the electronic part of the classical polarization of the bulk's unit cell, and the intercellular Zak phase γ^{inter} represents the difference between the net weight of the Wannier functions in the left and right sides of the 1D system with respect to a unit-cell boundary, with their centers belonging to opposite sides as illustrated in Fig. 1. We then show that in a terminated system this interpretation of the intercellular Zak phase leads to an accurate prediction of the extra charge accumulation (total charge including ionic contributions) in the surface regions. This is the essential result of our work, applicable to any translationally invariant insulator, that provides a bulk-boundary correspondence: There are $n_s = \gamma^{\text{inter}}/\pi$ (mod 2) surface modes below the Fermi level in a finite system if it is commensurate with an inversion-symmetric unit cell and γ^{inter} is evaluated from this commensurate unit cell. Our bulk-boundary correspondence resolves the above-mentioned subtle issues of the conventional bulk-boundary correspondence because γ^{inter} is independent of real-space origin while its unit-cell dependence is included in the commensurability condition.

The rest of the paper is organized as follows: In Secs. II and III we provide the physical meaning of the intracellular and intercellular Zak phases and show how they are related, respectively, to the electronic part of the classical polarization of the bulk and the extra charge accumulation in the surface region. In Sec. IV, based on this physical interpretation of the parts of the Zak phase, we develop a reformulated bulk-boundary correspondence of one-dimensional systems employing the intercellular Zak phase. In Sec. V we apply our interpretation of the intercellular Zak phase and the

bulk-boundary correspondence to the Rice-Mele 1D chain model and two 2D toy models which can be treated as effective 1D systems by fixing one of the momenta. Finally, discussions and concluding remarks are given in Sec. VI.

II. INTRACELLULAR AND INTERCELLULAR ZAK PHASE

Let us consider a general translationally invariant one-dimensional system described within the tight-binding approximation. The system consists of N_b atomic sites per unit cell, each with N_{orb}^i orbitals, including the spin degree of freedom for spinful systems. The ionic charge at site i is $Z_i e$, and the total ionic charge in the unit cell is $Ze = \sum_{i=1}^{N_b} Z_i e$. In order for the insulating system to be neutral, there are then necessarily Z fully filled bands below the Fermi level. Within the Born–von Karman boundary condition $\psi(x + Na) = \psi(x)$, the Bloch eigenfunctions of this system take the form

$$\psi_{n,k}(x) = \frac{1}{\sqrt{N}} \sum_m^N \sum_{i=1}^{N_b} \sum_{\zeta=1}^{N_{\text{orb}}^i} \alpha_k^{n,i,\zeta} \phi_m^{i,\zeta}(x) e^{ikma}, \qquad (4)$$

where N is the number of unit cells, and m and n are the unit cell and band index. Here,

$$\phi_m^{i,\zeta}(x) = \phi^\zeta(x - ma - b_i a) \qquad (5)$$

is the ζth atomic orbital centered at $ma + b_i a$ which is the position of the ith atomic site in the mth unit cell. Atomic orbitals at the same site are orthonormal and the overlaps between orbitals on different sites are assumed to be exponentially vanishing in accordance with the tight-binding condition [44]. The coefficients $\alpha_k^{n,i,\zeta}$ are obtained from solving the eigenvalue problem with the tight-binding Hamiltonian. We choose the gauge in which every atomic orbital in the mth unit cell has the same phase factor e^{ikma} in (4); the coefficients α then satisfy the periodic boundary condition $\alpha_{k+G}^{n,i,\zeta} = \alpha_k^{n,i,\zeta}$, where G is a reciprocal lattice vector [43]. In another widely used gauge, the phase factor for the orbitals at $ma + b_i a$ is instead given by $e^{ik(ma+b_i a)}$ [22,25,36,39,40]. In this case, the

same Bloch eigenfunction $\psi_{n,k}(x)$ is obtained by replacing the coefficient $\alpha_k^{n,i,\zeta}$ with $\tilde{\alpha}_k^{n,i,\zeta} = \alpha_k^{n,i,\zeta} e^{-ikb_ia}$, which satisfies the twisted boundary condition $\tilde{\alpha}_{k+G}^{n,i,\zeta} = \tilde{\alpha}_k^{n,i,\zeta} e^{-iGb_ia}$. While both gauges yield the same Zak phase, since they describe the same Bloch eigenfunction $\psi_{n,k}(x)$, the former allows for a natural separation of the Zak phase into the intracellular and intercellular parts.

The Zak phase, following Kudin *et al.* [43], can be split into two terms. The nth band Zak phase (2) is obtained from the lattice periodic part of the Bloch functionw

$$u_{n,k}(x) = \sqrt{N} e^{-ikx} \psi_{n,k}(x) \tag{6}$$

which satisfies the orthonormality condition $\langle u_{n,k}|u_{n,k'}\rangle = \int_\Omega dx\, u_{n,k}(x)^* u_{n,k'}(x) = \delta_{k,k'}$ [2]. The inner product $\langle u_{n,k}|\partial_k u_{n,k}\rangle$ in the Zak phase is defined as

$$\langle u_{n,k}|\partial_k u_{n,k}\rangle = \int_\Omega dx\, u_{n,k}^*(x)\frac{\partial}{\partial k} u_{n,k}(x), \tag{7}$$

with Ω a unit cell. Then, the Zak phase is split into the intracellular and intercellular Zak phase as

$$\gamma_n = \gamma_n^{\text{intra}} + \gamma_n^{\text{inter}}, \tag{8}$$

where

$$\gamma_n^{\text{intra}} = N \int_{\text{BZ}} dk \int_\Omega dx\, x|\psi_{n,k}(x)|^2 - 2\pi m_\Omega, \tag{9}$$

where m_Ω is the index of the unit cell Ω, and

$$\gamma_n^{\text{inter}} = i \sum_{i=1}^{N_b}\sum_{\zeta=1}^{N_{orb}^i} \int_{\text{BZ}} dk\, \alpha_k^{n,i,\zeta*}\frac{\partial}{\partial k}\alpha_k^{n,i,\zeta}. \tag{10}$$

(See Appendix A for further details.) Note that γ_n^{intra} depends on the real-space origin while γ_n^{inter} does not because $\alpha_k^{n,i,\zeta}$, being an element of the eigenvector of the momentum-space representation of the Hamiltonian, is origin independent.

To give a physical interpretation of the Zak phases just introduced, we start by relating the electronic part of the classical polarization of the unit cell to the intracellular Zak phase. We consider contributions from each filled band separately. For the nth band, we have

$$P_{n,\text{cl}}^{\text{el}} = \frac{1}{a}\int_\Omega dx\, x\rho_{\text{bulk},n}^{\text{el}}(x) \tag{11}$$

$$= -\frac{e}{a}\int_\Omega dx\, x\sum_{k\in\text{BZ}}|\psi_{n,k}(x)|^2 \tag{12}$$

$$= \frac{-e}{2\pi}\gamma_n^{\text{intra}} - m_\Omega e, \tag{13}$$

where $\rho_{\text{bulk},n}^{\text{el}}(x)$ is the electronic density corresponding to the nth band. That is, $P_{n,\text{cl}}^{\text{el}}$ can be evaluated from the intracellular Zak phase up to mod e.

Second, we give a physical interpretation of the intercellular Zak phase. To this end, we employ the Wannier functions given by

$$W_{n,m}(x) = \frac{1}{\sqrt{N}}\sum_{k\in\text{BZ}}\psi_{n,k}(x)e^{-ikma} \tag{14}$$

$$= \sum_{m'}^{N}\sum_{i=1}^{N_b}\sum_{\zeta=1}^{N_{orb}^i} A_{m'-m}^{n,i,\zeta}\phi_{m'}^{i,\zeta}(x), \tag{15}$$

where

$$A_{m'-m}^{n,i,\zeta} = \frac{1}{N}\sum_{k\in\text{BZ}}e^{ik(m'-m)a}\alpha_k^{n,i,\zeta}. \tag{16}$$

They satisfy the orthonormality condition $\langle W_{n,m}|W_{n',m'}\rangle = \delta_{n,n'}\delta_{m,m'}$. Note that in 1D the Wannier function $W_{n,m}(x)$ is in general guaranteed to be exponentially localized around a position in the mth unit cell [45–47] while, in 2D and 3D, this is true if and only if the Chern number of the band vanishes [48,49]. Then, we express the nth band intercellular Zak phase, via the inverse transformation of (16), as

$$\gamma_n^{\text{inter}} = 2\pi\sum_{m}^{N}\sum_{i=1}^{N_b}\sum_{\zeta=1}^{N_{orb}^i} m\left|A_m^{n,i,\zeta}\right|^2. \tag{17}$$

By fixing a point x_b at the boundary between neighboring unit cells, which we assume for concreteness to be between the $m = -1$ and 0 unit cells, the system is split into the left (L) and right (R) regions as depicted in Fig. 1. With these definitions, the intercellular Zak phase can be split into two parts as

$$\gamma_n^{\text{inter}} = -\gamma_n^{R\to L} + \gamma_n^{L\to R}, \tag{18}$$

where

$$\gamma_n^{R\to L} = -2\pi\sum_{m=-\infty}^{-1}\sum_{i=1}^{N_b}\sum_{\zeta=1}^{N_{orb}^i} m\left|A_m^{n,i,\zeta}\right|^2 \tag{19}$$

$$= 2\pi\sum_{m'=0}^{\infty}\int_{-\infty}^{x_b} dx\left|W_{n,m'}(x)\right|^2 \tag{20}$$

and

$$\gamma_n^{L\to R} = 2\pi\sum_{m=0}^{\infty}\sum_{i=1}^{N_b}\sum_{\zeta=1}^{N_{orb}^i} m\left|A_m^{n,i,\zeta}\right|^2 \tag{21}$$

$$= 2\pi\sum_{m'=-\infty}^{-1}\int_{x_b}^{\infty} dx|W_{n,m'}(x)|^2. \tag{22}$$

Further details are given in Appendix A. From (20) and (22), we note that

$$Q^{R\to L} = \sum_n^Z Q_n^{R\to L} = -\frac{e}{2\pi}\sum_n^Z \gamma_n^{R\to L} \tag{23}$$

represents the total charge weight in the L region of all Wannier functions with their centers belonging to the R region, and vice versa for $Q^{L\to R} = -e/(2\pi)\sum_n^Z \gamma_n^{L\to R}$. Finally, their difference in the L region is simply expressed by

$$\Delta Q^L = Q^{R\to L} - Q^{L\to R} = \frac{e}{2\pi}\sum_{n=1}^Z \gamma_n^{\text{inter}}, \tag{24}$$

where the sum is over the filled bands. In the R region, this difference is just given by $\Delta Q^R = -(e/2\pi)\sum_{n=1}^Z \gamma_n^{\text{inter}}$. Due to the translational symmetry of the system, this result is valid for any unit-cell boundary. Also, this quantity does not depend on the position of the origin since the intercellular Zak
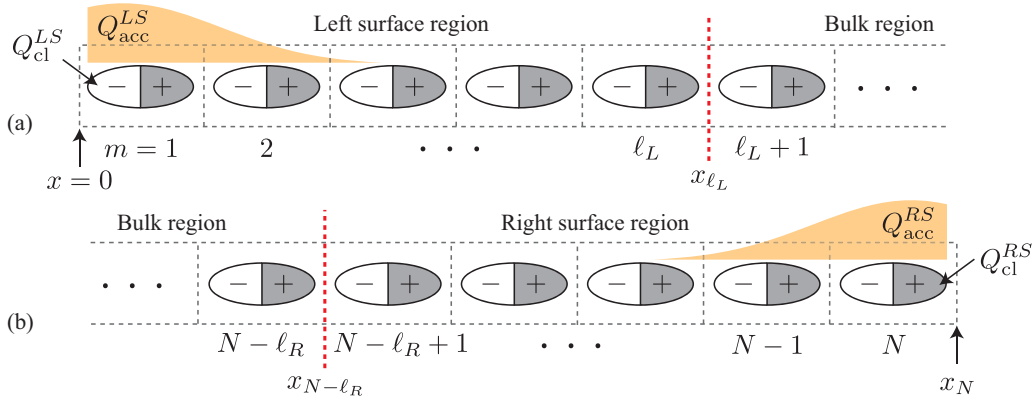
FIG. 2. A schematic of the three regions (bulk, left, and right surface regions) of a finite 1D system with N unit cells. Classical bound surface charges ($Q_{\text{cl}}^{LS\,(RS)} = \mathbf{P}_{\text{cl}} \cdot \hat{n}$) and extra charge accumulations ($Q_{\text{acc}}^{LS\,(RS)}$) in two surface regions are also illustrated schematically. The system is terminated at $x = 0$ and x_N. Boundaries between those three regions are represented by red dashed lines at x_{ℓ_L} and $x_{N-\ell_R}$. Bulk unit cells are drawn by gray dashed boxes and their indices are given below them. In each bulk unit cell, the dipole moment ($\mathbf{P}_{\text{cl}}$) of the bulk unit cell is drawn symbolically.

phase does not as mentioned previously. Note that, from the point of view of the electronic density of the infinite system without boundaries, every unit cell is neutral and there is no extra charge in the L and R regions of the bulk illustrated in Fig. 1. However, we want to eventually obtain the extra charge accumulation around the surfaces when the system is terminated as shown in Fig. 2; we demonstrate how it is related to $Q^{R \to L}$ and $Q^{L \to R}$ in the next section.

III. EXTRA CHARGE ACCUMULATIONS AROUND SURFACES

In this section, we consider a terminated system, divided into three regions as illustrated in Fig. 2: the left surface region (LS) from $m = 1$ to ℓ_L and the right surface (RS) region from $m = N - \ell_R + 1$ to N, separated by the bulk region (B) from $m = \ell_L + 1$ to $N - \ell_R$. We choose ℓ_L, ℓ_R, and N all large enough that there are no boundary effects in the bulk, and all regions are commensurate with the bulk's unit cell, namely, they do not contain any partial unit cells. While the extra charge accumulation in the surface region is defined as the additional charge over the bulk's charge distribution, it is equivalent to the total charge including ions in this region because of the commensurability condition and the neutrality of the bulk's unit cell. Finally, we assume that the finite system is also insulating because otherwise partially filled degenerate states at the Fermi level would yield ambiguity in evaluating physical quantities depending on which states we choose to be occupied. Then, we show that, if the surface region is commensurate with the bulk's unit cell, the extra charge accumulation $Q_{\text{acc}}^{LS\,(RS)}$ in the left (right) surface region of a neutral 1D insulator is given by

$$Q_{\text{acc}}^{LS\,(RS)} = +(-)\frac{e}{2\pi}\gamma^{\text{inter}} \ (\text{mod } e) \tag{25}$$

where $\gamma^{\text{inter}} = \sum_{n=1}^{Z} \gamma_n^{\text{inter}}$ is evaluated based on the commensurate unit cell.

The overall strategy for the demonstration of the relation (25) is as follows. We prepare a set of orthonormal wave

functions that are related to the set of occupied eigenfunctions of the finite system by a unitary transformation, following Vanderbilt *et al.* [4]. All of these states are localized, i.e., Wannier type, such that their characteristic widths are much smaller than sizes of the three regions. First, there are exchanges of weights of the Wannier functions between the surface and bulk regions across their boundary as expressed by ΔQ^L and ΔQ^R in the previous section. Then, from the orthonormality and localized feature of the prepared basis set, we show that the total charge in the left and right surface regions should be ΔQ^L and ΔQ^R modulo e.

The orthonormal localized wave functions that we employ for the description of the terminated system are given by

$$\boldsymbol{\varphi} = \big\{\varphi_1^{LS}(x), \ldots, \varphi_{s_L}^{LS}(x), W_{1,m_L}(x), \ldots, W_{Z,m_R}(x),$$
$$\varphi_1^{RS}(x), \ldots, \varphi_{s_R}^{RS}(x)\big\}^{\text{T}}. \tag{26}$$

While the Wannier functions are the proper basis set for the infinite system, after the termination we need to construct this new set of basis wave functions that satisfy the open boundary condition. $\boldsymbol{\varphi}$ span the same Hilbert space as the M occupied eigenstates of the terminated system denoted by $\boldsymbol{\psi}^{\text{t.s.}}(x) = \{\psi_1^{\text{t.s.}}(x), \ldots, \psi_M^{\text{t.s.}}(x)\}^{\text{T}}$ [4]. First, we pick all occupied Wannier functions from the unit cell m_L (in the left surface region) to m_R (in the right surface region). The choice of m_L and m_R is arbitrary but chosen to be far enough from the surfaces so that corresponding Wannier functions satisfy the boundary conditions with exponentially vanishing error. We then replace the Wannier functions around the surfaces with another set of wave functions that satisfy the open boundary condition; these we denote by $\varphi_s^{LS}(x)$ and $\varphi_s^{RS}(x)$ around the left and right boundary each. The set of wave functions in (26) can always be made orthonormal through the Gram-Schmidt orthonormalization process [4,50–52].

The charge density of the occupied electrons in the terminated system is given by $\rho_{\text{t.s.}}^{\text{el}}(x) = -e\boldsymbol{\psi}^{\text{t.s.}}(x)^{\dagger}\boldsymbol{\psi}^{\text{t.s.}}(x)$. Since $\boldsymbol{\psi}^{\text{t.s.}}(x)$ and $\boldsymbol{\varphi}(x)$, as orthonormal bases, span the same Hilbert space of occupied states, they are related by a unitary

matrix, and the electronic charge is rewritten as

$$\rho_{\text{t.s.}}^{\text{el}}(x) = -e\boldsymbol{\varphi}(x)^\dagger \boldsymbol{\varphi}(x) \tag{27}$$

$$= -e\left(\sum_s^{s_L} \left|\varphi_s^{LS}(x)\right|^2 + \sum_s^{s_R} \left|\varphi_s^{RS}(x)\right|^2 \right.$$

$$\left. + \sum_{n=1}^{Z} \sum_{m=m_L}^{m_R} |W_{n,m}(x)|^2 \right). \tag{28}$$

The total charge in the left surface region, which is the extra charge accumulation, is then evaluated as

$$Q_{\text{acc}}^{LS} = \int_0^{x_{\ell_L}} dx\, \rho_{\text{t.s.}}^{\text{el}}(x) + \ell_L Z e, \tag{29}$$

where $\ell_L Z e$ is the total ionic charge in the left surface region: we assume that the left end of the system is at $x = 0$ and $x_m = am$ is the position of the right boundary of the mth unit cell. In this region, integrals of $\varphi_s^{RS}(x)$'s in (28) vanish, while the sum of integrals of $\varphi_s^{LS}(x)$'s, which are well localized to the right and left surface, is an integer number s_L. Then, Q_{acc}^{LS} becomes

$$Q_{\text{acc}}^{LS} = -e\int_0^{x_{\ell_L}} dx \sum_{n=1}^{Z} \sum_{m=m_L}^{m_R} |W_{n,m}(x)|^2 + q_L e \tag{30}$$

$$= -e\sum_{n=1}^{Z} \sum_{m=m_L}^{\ell_L} \int_0^{x_{\ell_L}} dx |W_{n,m}(x)|^2$$

$$- e\sum_{n=1}^{Z} \sum_{m=\ell_L+1}^{m_R} \int_0^{x_{\ell_L}} dx |W_{n,m}(x)|^2 + q_L e, \tag{31}$$

where $q_L = -s_L + \ell_L Z$. Since all the Wannier functions are normalized, we have the identity

$$\sum_{n=1}^{Z} \sum_{m=m_L}^{\ell_L} \int_0^{x_{\ell_L}} dx |W_{n,m}(x)|^2$$

$$= Z(\ell_L - m_L + 1) - \sum_{n=1}^{Z} \sum_{m=m_L}^{\ell_L} \int_{x_{\ell_L}}^{x_N} dx |W_{n,m}(x)|^2. \tag{32}$$

This leads to the conclusion

$$Q_{\text{acc}}^{LS} = \frac{-e}{2\pi} \sum_{n=1}^{Z} \left(\gamma_n^{R\to L} - \gamma_n^{L\to R} \right) + q_L' e \tag{33}$$

$$= \frac{e}{2\pi} \sum_{n=1}^{Z} \gamma_n^{\text{inter}} + q_L' e, \tag{34}$$

where $q_L' = q_L - Z(\ell_L - m_L + 1) = -s_L + Z(m_L - 1)$. When we apply (20) and (22) to (31) and (32), we take $m_L \to -\infty$, $m_R \to \infty$, $x_1 \to -\infty$, and $x_N \to \infty$, which is an approximation justified by the fact that the Wannier functions are exponentially localized in space and that the surface regions can be taken large enough. Also, the role of x_b in (20) and (22) is taken by x_{ℓ_L} in (31) and (32). In the same way, the extra charge accumulation in the right surface region

is given by

$$Q_{\text{acc}}^{RS} = -\frac{e}{2\pi} \sum_{n=1}^{Z} \gamma_n^{\text{inter}} + q_R' e, \tag{35}$$

where $q_R' = -s_R + Z(N - m_R)$. As in Ref. [4], we are not interested in the integer numbers q_L' and q_R' which cannot be determined from the bulk. Instead, we conclude that the intercellular Zak phase can predict the extra charge accumulation in the surface region modulo e as described in (25).

Finally, we remark on the difference between the bound surface charge and the extra charge accumulation. The bound surface charge σ is a quantity measured in a capacitance measurement and is related to the modern definition of the polarization by $\sigma = \mathbf{P} \cdot \hat{n}$, where $\hat{n}$ is the surface orientation [$\hat{n} = - (+)\hat{x}$ for the left (right) edge in the 1D case] [4]. The bound surface charge of the total charge density $\rho_{\text{t.s.}}(x)$ of the finite system is evaluated explicitly as [4,53,54]

$$\sigma^{LS} = \frac{1}{a} \int_{-\infty}^{x_c} dx \int_{x-\frac{a}{2}}^{x+\frac{a}{2}} dx' \rho_{\text{t.s.}}(x') \tag{36}$$

for the bound surface charge at the left edge, and

$$\sigma^{RS} = \frac{1}{a} \int_{x_d}^{\infty} dx \int_{x-\frac{a}{2}}^{x+\frac{a}{2}} dx' \rho_{\text{t.s.}}(x') \tag{37}$$

at the right edge, where x_c and x_d are arbitrary positions in the middle of the finite system far away from the surfaces. As shown in Appendix B, σ^{LS} and σ^{RS} are independent of x_c and x_d. To clearly compare the bound surface charge and the extra charge accumulation, we choose them as $x_c = x_{\ell_L} + a/2$ and $x_d = x_{N-\ell_R} - a/2$. Then, the left and right bound surface charges become

$$\sigma^{LS} = -\frac{1}{a} \int_{x_{\ell_L}}^{x_{\ell_L}+a} dx\, x\rho_{\text{t.s.}}(x) + \int_0^{x_{\ell_L}} dx\, \rho_{\text{t.s.}}(x) \tag{38}$$

and

$$\sigma^{RS} = \frac{1}{a} \int_{x_{N-\ell_R}-a}^{x_{N-\ell_R}} dx\, x\rho_{\text{t.s.}}(x) + \int_{x_{N-\ell_R}}^{x_N} dx\, \rho_{\text{t.s.}}(x). \tag{39}$$

Derivations of the above are given in Appendix B. The first terms of (38) and (39) are exactly $\mathbf{P}_{\text{cl}} \cdot \hat{n}$ because x_{ℓ_L} and $x_{N-\ell_R}$ are far enough from the edges so that $\rho_{\text{t.s.}}(x)$ can be considered a bulk charge density. We call them the *classical bound surface charges* $Q_{\text{cl}}^{LS\,(RS)}$ because in classical electrodynamics they are the bound surface charges in a dielectric material with a uniform dipole distribution through the whole finite system. On the other hand, the second terms of (38) and (39) are just the total charge in the left and right surface regions, which are equal to the extra charge accumulations in those regions in the neutral systems. Consequently, we have shown that the bound surface charge consists of two contributions, one from the bulk's dipole moment and the other from the extra charge accumulation. This is consistent with the splitting of the Zak phase into the intracellular and intercellular Zak phases. Also, it indicates that the modern polarization is actually composed of two kinds of polarizations: one is the classical one from the bulk's dipole moment and the other is polarization from the

extra charge accumulations at opposite edges. This conclusion is illustrated schematically in Fig. 2.

IV. BULK-BOUNDARY CORRESPONDENCE

Our general statement about the number of surface modes in the gap of a finite 1D insulator with charge neutrality is as follows: there are $n_s = \gamma^{\text{inter}}/\pi$ (mod 2) surface modes below the Fermi level if there is inversion symmetry both before and after termination, and the finite system is commensurate with the bulk unit cell used for the calculation of γ^{inter}. We justify our general statement in the light of the physical interpretation of the intercellular Zak phase γ^{inter}. As discussed in the previous section, the intercellular Zak phase explains the amount of the extra charge accumulation around the edge which is closely related to the surface modes, while the intracellular Zak phase, as a bulk dipole moment, has nothing to do with the surface modes.

First, we note that if the bulk respects inversion symmetry, γ^{inter} is quantized to π. When the real-space origin is at one of the inversion centers, the total Zak phase γ is quantized to π while its intracellular part vanishes because the dipole moment of the bulk unit cell is zero in this case. Therefore, $\gamma^{\text{inter}} = \gamma$ is also quantized to π, and it is independent of the choice of the origin as mentioned in Sec. II.

The surface modes are the eigenstates generated in the bulk gaps as a result of the edge termination. As described in the previous section, they are exponentially localized at one of the edges. Due to inversion symmetry, if we have a surface state localized at the left edge, we always find its counterpart localized at the right edge with the same energy. The degeneracy might increase if the system preserves additional symmetries such as the time-reversal symmetry.

We proceed to the justification of our general statement by examining two different cases. One is when the Fermi level of the finite system is not at any of the surface modes, so that the finite system is also an insulator. And, the other is the case when the Fermi level is at the partially filled degenerate surface modes.

First, let us consider the case when the finite system is already insulating. Then, the only allowed value of the total charge accumulations is $Q_{\text{acc}}^{LS} = Q_{\text{acc}}^{RS} = 0$ due to charge neutrality and inversion symmetry. According to (25), the intercellular Zak phase should be 0 (mod 2π) in this case. Since every surface mode has an inversion partner with the same energy, there should be an even number of surface states below the Fermi level. This means the general statement holds for insulating phases with inversion symmetry.

Second, we consider the case when the Fermi level is located at the surface modes. In this case, we cannot use the results of the previous section since there we assume the finite system is insulating. However, we can resolve this obstacle by opening tiny gaps between degenerate surface modes without changing the total number of surface modes in the bulk gap. We assume that this can be done by applying local perturbative potentials on both edges that break symmetries corresponding to those degeneracies. For instance, different onsite potentials at opposite edges would break the degeneracy responsible for inversion symmetry. Similarly, a local Zeeman field could be used to break spin degeneracy.

Let us investigate the dependence of the surface modes on the tiny inversion-symmetry breaking, which is relevant for the quantization of the extra charge accumulations on the edges as explained below. This is achieved by applying an onsite potential δ to the first unit cell and $-\delta$ to the Nth unit cell of the finite system where δ is nonzero but small compared with the bulk gap. Then, the eigenstates at opposite edges have different energies, and it is impossible to construct surface modes localized to both edges simultaneously from them. As a result, the eigenstate of each lifted surface mode is localized to only one of the left and right edges. This implies that each surface mode yields an integer charge $Q_{S_i,\text{acc}}^{LS} = -e$ or $Q_{S_i,\text{acc}}^{RS} = -e$, where $Q_{S_i,\text{acc}}^{LS(RS)}$ is the contribution of the ith surface mode to the extra charge accumulation in the left (right) surface region. After taking into account the inversion-symmetry breaking, we assume that other perturbative potentials would not affect this property of the lifted surface modes.

On the other hand, the charge distribution calculated from the bulk band continuum is insensitive against this kind of local perturbation due to its bulk character [55]. So, the charge distribution of the bulk band continuum maintains almost the same form as the unperturbed inversion-symmetric system. In the unperturbed inversion-symmetric system, the extra charge accumulation from the bulk band continuum can only take values of $Q_{B,\text{acc}}^{LS} = Q_{B,\text{acc}}^{RS} = (p + 1/2)e$ or pe where p is an integer because the total charge of the finite system should be an integer multiple of e and the system has inversion symmetry. Here, $Q_{B,\text{acc}}^{LS(RS)}$ is the contribution of the bulk band continuum to the extra charge accumulation in the left (right) surface region. Note that although we slightly break the inversion symmetry to make the system insulating, its presence in the unperturbed system is essential for the constraint on $Q_{B,\text{acc}}^{LS(RS)}$.

If $Q_{B,\text{acc}}^{LS(RS)} = (p + 1/2)e$, the total charge accumulations originating from surface modes on both sides should be $\sum_{E_i < E_F} (Q_{S_i,\text{acc}}^{LS} + Q_{S_i,\text{acc}}^{RS}) = -(2p + 1)e$ to maintain neutrality. This means that there is an odd number of surface modes below the Fermi level in the main gap where the Fermi level lies because there were even number of occupied surface modes in other gaps before breaking inversion symmetry, and we have assumed that this number is unchanged by the symmetry-breaking perturbations. Also, due to the same reason, this implies that we have an odd number of surface modes below the Fermi energy in the main gap before breaking those symmetries. In the perspective of the intercellular Zak phase, the fact that the extra charge accumulation $Q_{B,\text{acc}}^{LS(RS)} + \sum_{E_i < E_F} Q_{S_i,\text{acc}}^{LS(RS)}$ is a half-integer multiple of e implies that the intercellular Zak phase should be a half-integer multiple of 2π according to (25). In conclusion, the number of surface modes is equal to $\gamma^{\text{inter}}/\pi$ mod 2 in this case.

In similar fashion, when $Q_{B,\text{acc}}^{LS(RS)} = pe$, the surface modes' extra charge accumulations on both edges should be $\sum_{E_i < E_F} (Q_{S_i,\text{acc}}^{LS} + Q_{S_i,\text{acc}}^{RS}) = -2pe$ to maintain charge neutrality, implying that there are an even number of surface modes in the main gap and that the intercellular Zak phase is even. So, the number of surface modes is again equal to $\gamma^{\text{inter}}/\pi$ mod 2 in this case.

Finally, we note that this bulk-boundary correspondence can be restated by using the Zak phase when the real-space origin is at an inversion center. This is because the intracellular

Zak phase becomes zero (mod 2π) according to (9), so that the Zak phase is identical to the intercellular Zak phase in this case.

V. EXAMPLES

In this section, we provide a few examples demonstrating the general results of the earlier sections.

A. Rice-Mele 1D chain

In this section, we calculate the extra charge accumulation in the Rice-Mele model [4,56] and show that it is accurately predicted by the intercellular Zak phase and is different from the bound surface charge. Also, for inversion-symmetric cases of this model, we show that the bulk-boundary correspondence works well.

The Rice-Mele model is given by

$$\mathcal{H}_{\mathrm{RM}} = \sum_{\sigma,j} \epsilon_j c_{\sigma j}^\dagger c_{\sigma j} + \sum_{\sigma,j} [V_{j,j+1} c_{\sigma j}^\dagger c_{\sigma j+1} + \mathrm{H.c.}], \quad (40)$$

where σ and j are indices for the spin and the lattice sites. For neutrality of the system at half-filling, we introduce spin degeneracy. The tight-binding parameters are given by $\epsilon_{2p} = -\Delta$, $\epsilon_{2p+1} = \Delta$, $V_{2p-1,2p} = -t - \delta$, and $V_{2p,2p+1} = -t + \delta$ where p is an integer. Note that there are two sites per unit cell. When $\Delta = 0$, the model reduces to the Su-Schrieffer-Heeger model [57].

The Bloch wave function for $\mathcal{H}_{\mathrm{RM}}$ is described by

$$\psi_{n,k}(x) = \frac{1}{\sqrt{N}} \sum_m^N e^{ikm} \left[\alpha_{n,k} \phi_m^A(x) + \beta_{n,k} \phi_m^B(x) \right], \quad (41)$$

where

$$\phi_m^A(x) = \phi(x - m) \text{ and } \phi_m^B(x) = \phi\left(x - m - \tfrac{1}{2}\right) \quad (42)$$

and $\phi(x)$ is the atomic wave function at the lattice sites. In this section, we set $a = 1$ for convenience.

The intracellular and intercellular Zak phases are given by

$$\gamma_{n,\sigma}^{\mathrm{intra}} = \int_0^{2\pi} dk \frac{1}{2} |\beta_{n,k}|^2 \quad (43)$$

and

$$\gamma_{n,\sigma}^{\mathrm{inter}} = i \int_0^{2\pi} dk \left(\alpha_{n,k}^* \frac{\partial \alpha_{n,k}}{\partial k} + \beta_{n,k}^* \frac{\partial \beta_{n,k}}{\partial k} \right). \quad (44)$$

Since there are no couplings between the two spin species, we have $\gamma_{n,\uparrow} = \gamma_{n,\downarrow}$. According to the results in Sec. II, the classical polarization for a given unit cell is

$$P_{\mathrm{cl}} = \frac{-e}{2\pi} \sum_\sigma \sum_{n=1}^Z \gamma_{n,\sigma}^{\mathrm{intra}} + \frac{e}{2} \quad (45)$$

and the extra charge accumulations at the edges are

$$Q_{\mathrm{acc}}^{LS\,(RS)} = +(-)\frac{e}{2\pi} \sum_\sigma \sum_{n=1}^Z \gamma_{n,\sigma}^{\mathrm{inter}} \pmod{2e}. \quad (46)$$

Here, $Z = 1$ since we consider two spins independently.

We check this relation between $Q_{\mathrm{acc}}^{LS\,(RS)}$ and the intercellular Zak phase numerically in Fig. 3(b) where the system
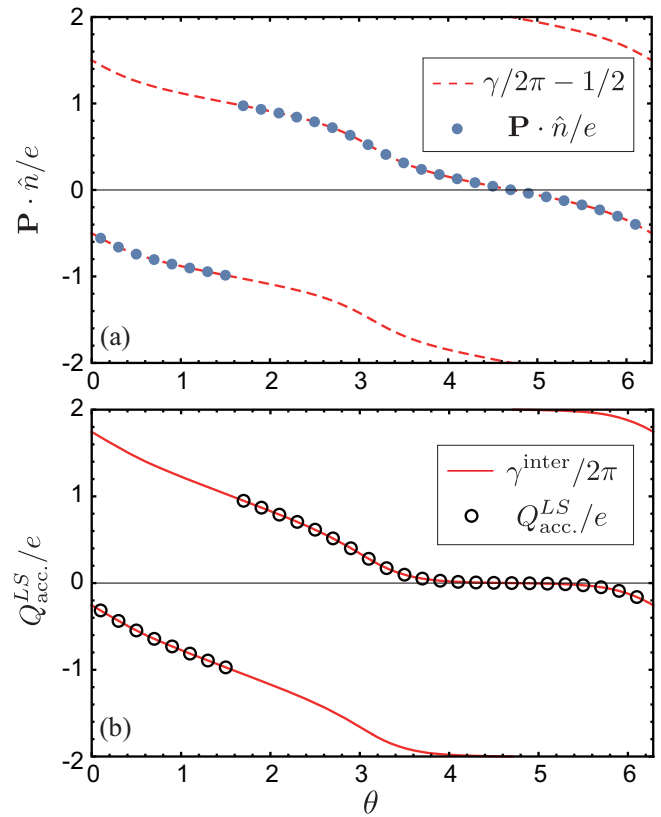

FIG. 3. The comparison between the Zak phase, the intercellular Zak phase, the bound surface charge, and the extra charge accumulation of the Rice-Mele 1D chain model. Here, the tight-binding parameters are given by $t = 1$, $\Delta = 0.6\cos\theta$, and $\delta = 0.6\sin\theta$. (a) The red dashed curves are the calculations of $\gamma/2\pi - 1/2$ (mod $2e$). The blue dots are the bound surface charge at the left edge of the terminated chain. (b) The red solid curves are the intercellular Zak phase and the circular markers are the extra charge accumulation near the left edge.

is parametrized by $t = 1$, $\Delta = 0.6\cos\theta$, and $\delta = 0.6\sin\theta$. Also, for the bound surface charge ($\sigma = \mathbf{P} \cdot \hat{n}$), we applied the formulas [53,54] (36) and (37) and reproduced exactly the results obtained by Vanderbilt *et al.* [4] as shown in Fig. 3(a). The difference between those two quantities corresponds to the classical bound surface charge $\sigma_{\mathrm{cl}} = \mathbf{P}_{\mathrm{cl}} \cdot \hat{n}$ originating from the dipole moment of the unit cell as we discussed in Sec. III. Since the dipole moment vanishes when the unit cell respects inversion symmetry, those two quantities become identical to each other at $\theta = \pi/2$ and $3\pi/2$ where $\Delta = 0$ as shown in Fig. 3.

As in Fig. 3(b), the intercellular Zak phase becomes 2π for $\theta = \pi/2$ and zero for $\theta = 3\pi/2$, which predicts an even number of surface bands below the Fermi level according to the bulk-boundary correspondence in the previous section. In the finite system with an even number of sites, we find two surface bands for $\theta = \pi/2$ and no surface bands for $\theta = 3\pi/2$ below the Fermi energy (data not shown), consistent with the bulk-boundary correspondence. However, if we consider two spins separately, we have more information. For each spin species, the intercellular Zak phase is just the half of those in Fig. 3(b), namely, π for $\theta = \pi/2$ and zero for $\theta = 3\pi/2$,
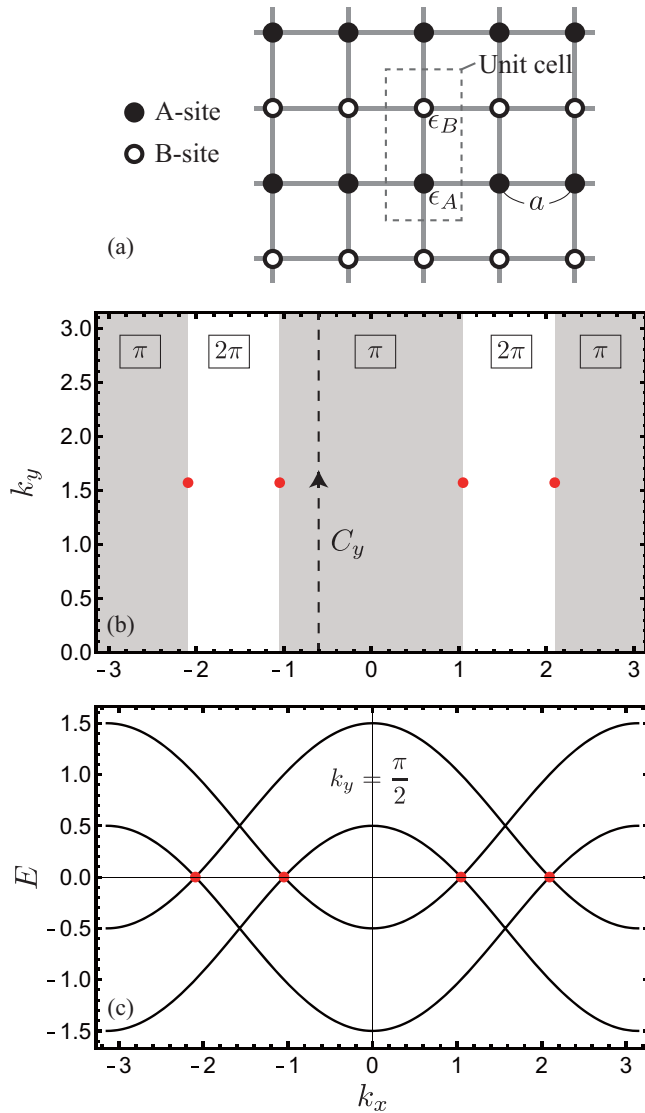
FIG. 4. The lattice structure of the 2D toy model-I. The unit cell used for the calculations of the intercellular Zak phases is the dashed box. (b) The Brillouin zone of the given system. Four Dirac nodes at $k_y = \pi/2$ are marked by red dots. The Brillouin zone is divided into several regions depending on the value of the Zak phase: $\gamma = \pi$ is gray and $\gamma = 2\pi$ is white. (c) Band spectrum at $k_y = \pi/2$. The parameters used are $t = \epsilon_0 = 0.5$.

which implies there are an odd and even number of surface states in each case. This means we must have surface modes when $\theta = \pi/2$ while one cannot determine the existence of the surface bands when $\theta = 3\pi/2$.

B. 2D toy model-I

Here, we suggest a 2D toy model as a counterexample for the conventional bulk-boundary correspondence of the Zak phase. From this, we clarify its right usage by emphasizing the assumption of the existence of the commensurate bulk's unit cell. We also test whether the intercellular Zak phase predicts the extra charge accumulation accurately or not.

Our toy model-I is illustrated in Fig. 4(a) and described by the Hamiltonian

$$\mathcal{H}_{2D}^{I} = \sum_{\mathbf{R},i}(\epsilon_A a_{i,\mathbf{R}}^{\dagger} a_{i,\mathbf{R}} + \epsilon_B b_{i,\mathbf{R}}^{\dagger} b_{i,\mathbf{R}})$$
$$+ t \sum_{\mathbf{R},\boldsymbol{\delta}_x}\left(a_{2,\mathbf{R}+\boldsymbol{\delta}_x}^{\dagger} a_{1,\mathbf{R}} + b_{2,\mathbf{R}+\boldsymbol{\delta}_x}^{\dagger} b_{1,\mathbf{R}} + \text{H.c.}\right)$$
$$+ t \sum_{\mathbf{R},\boldsymbol{\delta}_y}\left(a_{1,\mathbf{R}+\boldsymbol{\delta}_y}^{\dagger} b_{1,\mathbf{R}} - a_{2,\mathbf{R}+\boldsymbol{\delta}_y}^{\dagger} b_{2,\mathbf{R}} + \text{H.c.}\right), \quad (47)$$

where $\mathbf{R}$ is the position vector of the unit cell, and $\boldsymbol{\delta}_x = \pm a\hat{x}$ and $\boldsymbol{\delta}_y = \pm a\hat{y}$ are the nearest-neighbor vectors. There are two orbitals at each site denoted by $i = 1,2$. The electron hops between different orbitals along x and between the same orbitals along y. Along the y direction, the signs of the hopping parameter of the $i = 1$ and 2 orbitals are opposite.

For $\epsilon_A = -\epsilon_B = \epsilon_0$, the energy spectrum is given by

$$E_{2D}^{I}(k_x,k_y) = \pm\{(\epsilon_0 \pm 2t\cos k_x)^2 + 4t^2\cos^2 k_y\}^{\frac{1}{2}}, \quad (48)$$

where a is set to be unity. The spectrum can become gapless only at $k_y = \pi/2$, where it becomes $E_{2D}^{I}(k_x,\pi/2) = \pm(\epsilon_0 \pm 2t\cos k_x)$ which has four Dirac nodes at $k_x = \pm\cos^{-1}(\pm\epsilon_0/2t)$ for $0 < \epsilon_0 < 2t$ as shown in Figs. 4(b) and 4(c) where $t = \epsilon_0 = 0.5$.

For the Zak phase analysis, we consider an effective 1D Hamiltonian obtained by fixing the momentum k_x. From this, we can calculate the Zak phase by integrating the Berry connection along k_y. The results are presented in Fig. 4(b) by the gray ($\gamma = \pi$) and white ($\gamma = 2\pi$) regions. Due to reflection symmetry, which corresponds to inversion symmetry in the effective Hamiltonian, we have quantized Zak phases. Whenever we cross one of the Dirac nodes, the Zak phase changes discontinuously by $\pm\pi$.

Now, let us consider ribbon-shaped finite systems that are finite in the y direction but infinite in the x direction. We consider two kinds of ribbon geometries, which we call Ribbon-I(A) and Ribbon-I(S) as illustrated in the insets of Figs. 5(b) and 5(c). Ribbon-I(A) does not respect reflection symmetry along the x axis while Ribbon-I(S) does. As a result, only Ribbon-I(S) remains gapless without breaking the Dirac nodes of the bulk.

According to the conventional bulk-boundary correspondence, we expect Ribbon-I(S) to have surface modes at k_x's in the gray or white region in Fig. 4(b) because both the bulk and terminated system have reflection symmetry. However, it turns out that there are no boundary modes in the Brillouin zone for both ribbon geometries as shown in Fig. 5. This is a good example of the wrong usage of the bulk-boundary correspondence using the Zak phase. In the revised correspondence given in the previous section, it requires the commensurability between the finite system and the bulk's unit cell in addition to inversion symmetry. Ribbon-I(A) is commensurate with the unit cell described in Fig. 4(a), but does not respect mirror symmetry while Ribbon-I(S), which is reflection symmetric, cannot be commensurate with any bulk's unit cell as it consists of an odd number of dimer lines. Therefore, those two systems are actually beyond the scope of the revised bulk-boundary correspondence.
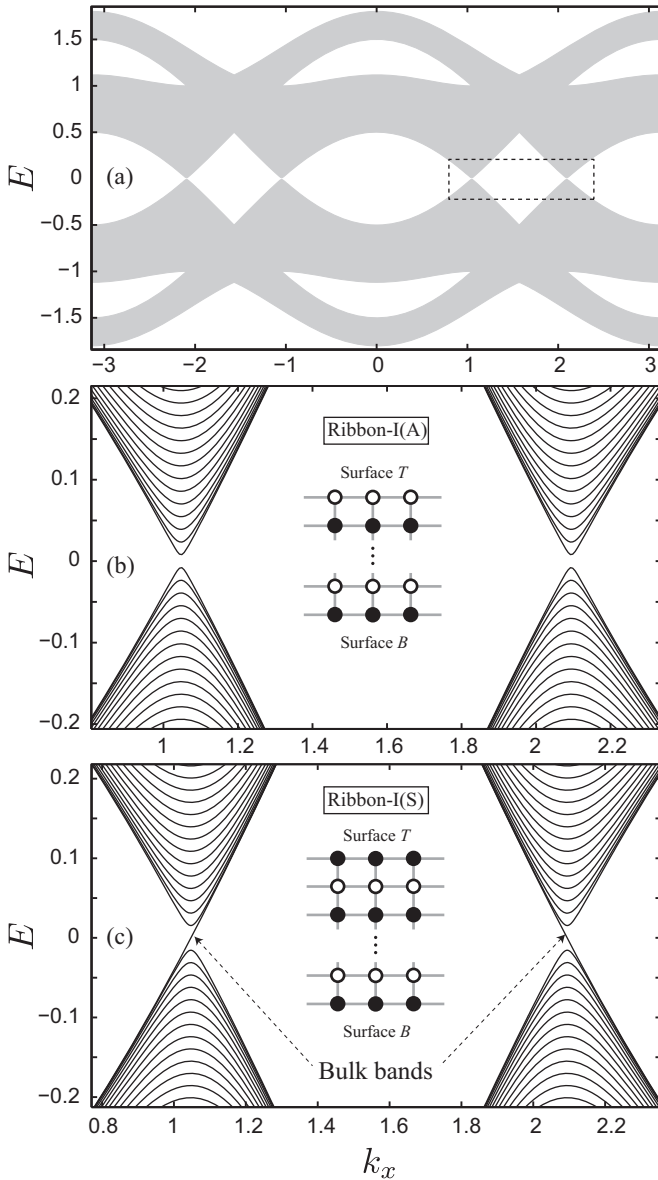
FIG. 5. (a) A schematic band dispersion of the terminated system of the 2D toy model-I. The dashed box in (a) is highlighted in (b) and (c) for different choices of the terminations, Ribbon-I(A) and Ribbon-I(S) each whose lattice structures are depicted in the insets of (b) and (c). Those ribbon geometries are infinite only along the x axis. Their bottom and top surfaces are denoted by surfaces B and T.

We check that the intercellular Zak phase accurately predicts the extra charge accumulation in the surface regions in Fig. 6. From (25), the extra charge accumulation for a given k_x is given by

$$Q_{\text{acc.}}^{B\,(T)}(k_x) = \pm \frac{e}{2\pi} \sum_n \gamma_n^{\text{inter}}(k_x)\,(\text{mod } e), \qquad (49)$$

where $B\,(T)$ and the plus (minus) sign correspond to the bottom (top) surface, and the sum is over occupied bands. In the case of Ribbon-I(A), both bottom and top surfaces are commensurate with a single unit cell and share the same intercellular Zak phase. As a result, the extra charge accumulations in the bottom and top surfaces show opposite
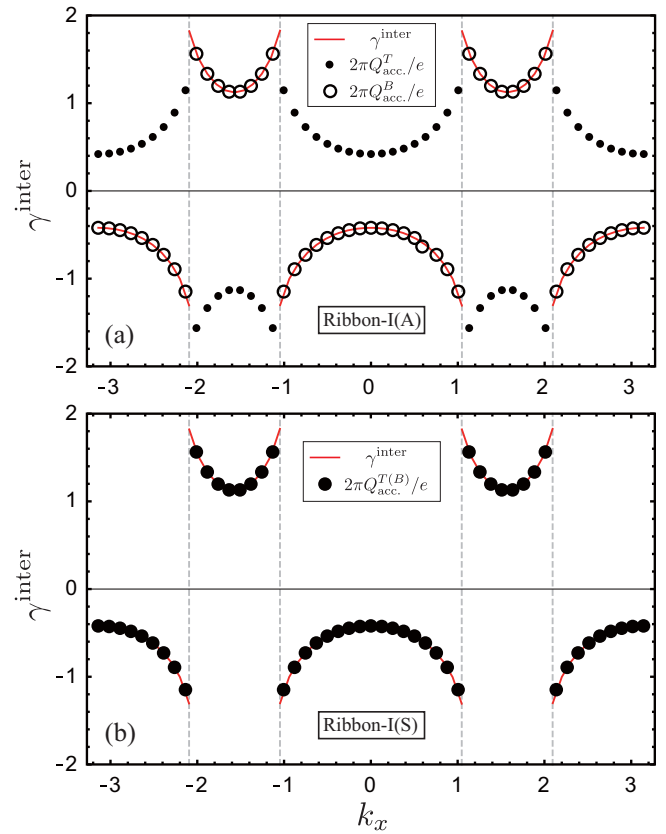

FIG. 6. The intercellular Zak phase ($\gamma^{\text{inter}} = \sum_n \gamma_n^{\text{inter}}$) is plotted by red solid curves as a function of k_x and it is compared with the extra charge accumulation which is represented by empty and filled circular markers. In (a), the empty (filled) circles are $2\pi\,Q_{\text{acc.}}^B/e$ ($2\pi\,Q_{\text{acc.}}^T/e$) of Ribbon-I(A). In (b), the filled circles represent the densities of the extra charge accumulations on both sides of Ribbon-I(S). In this case, the extra charge accumulations on both surfaces are the same due to reflection symmetry.

signs to each other as shown in Fig. 6(a). On the other hand, for Ribbon-I(S), the commensurate unit cell for the top surface is the one obtained by shifting the commensurate unit cell for the bottom by $a\hat{y}$. We find that the intercellular Zak phases for those unit cells have the same magnitude but opposite signs. While the extra charge accumulations in the bottom and top surfaces should be identical due to the mirror symmetry, it is consistent with the above property of intercellular Zak phases. This is described in Fig. 6(b).

C. 2D toy model-II

Finally, we study another 2D toy model which manifests the vitalness of the conditions for the bulk-boundary correspondence, such as inversion symmetry and insulating terminated system. We again confirm that the extra charge accumulation in the surface regions is captured by the intercellular Zak phase.

The toy model-II, depicted in Fig. 7(a), has a tight-binding model given by

$$\mathcal{H}_{\text{2D}}^{\text{II}} = \sum_{\mathbf{R}} \mathbf{c}_{\mathbf{R}}^\dagger H_0 \mathbf{c}_{\mathbf{R}} + \sum_{\mathbf{R},\boldsymbol{\delta}_x} \mathbf{c}_{\mathbf{R}+\boldsymbol{\delta}_x}^\dagger H_x \mathbf{c}_{\mathbf{R}} + \sum_{\mathbf{R},\boldsymbol{\delta}_y} \mathbf{c}_{\mathbf{R}+\boldsymbol{\delta}_y}^\dagger H_y \mathbf{c}_{\mathbf{R}},$$
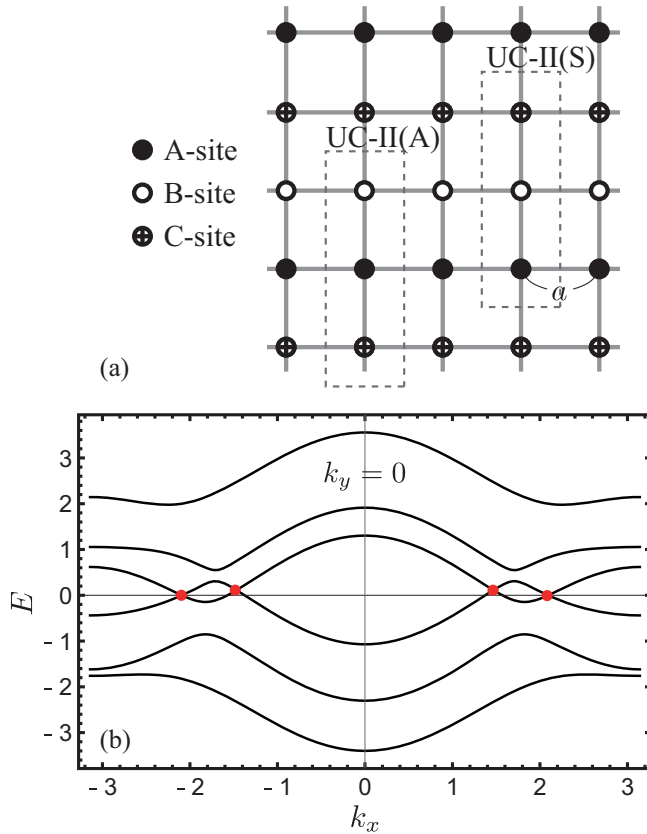
$$(50)$$

FIG. 7. (a) The lattice structure of the 2D toy model-II. Two unit-cell choices for the evaluation of the intercellular Zak phase are shown by two dashed boxes. (b) The band structure at $k_y = 0$ for $t = 0.5$ and $H_0 = \text{diag}(0.5, -1.5, 2, 0, 0.5, -1.5)$. Four Dirac points are represented by red dots.

where $\mathbf{c}_{\mathbf{R}}^{\dagger} = (a_{1,\mathbf{R}}^{\dagger}, a_{2,\mathbf{R}}^{\dagger}, b_{1,\mathbf{R}}^{\dagger}, b_{2,\mathbf{R}}^{\dagger}, c_{1,\mathbf{R}}^{\dagger}, c_{2,\mathbf{R}}^{\dagger})$ consists of the creation operators of the orbitals at A, B, and C sites. There are two orbitals per site. The matrices are defined as $H_0 = \text{diag}(\epsilon_{A,1}, \epsilon_{A,2}, \epsilon_{B,1}, \epsilon_{B,2}, \epsilon_{C,1}, \epsilon_{C,2})$, $H_x = \mathbb{1} \otimes (\sigma^x + \sigma^z)$, and $H_y = (\lambda_1 + \lambda_6) \otimes \sigma_z$, where $\mathbb{1}$ is the 3×3 identity matrix, σ^{α} is the Pauli matrix, and λ_i is the Gellman matrix. The band structure at $k_y = 0$ is depicted in Fig. 7(b). While there are four Dirac points at $k_y = 0$, as marked by red dots, it is insulating otherwise. We consider this model because we can investigate a finite system with both reflection symmetry and commensurate bulk's unit cell as shown below.

As in the previous 2D toy model-I, we consider the effective 1D Hamiltonian for a fixed k_x and calculate the intercellular Zak phases by integrating the Berry connection along the k_y axis. While γ^{inter} depends on the choice of the unit cell, we consider the two unit cells, called UC-II(A) and UC-II(S), illustrated in Fig. 7(a). Here, we assume that $\epsilon_{A,i} = \epsilon_{C,i}$ so that UC-II(S) preserves reflection symmetry while UC-II(A) does not. Calculations of γ^{inter} are shown in Fig. 8 by red solid curves along k_x. The intercellular Zak phase of UC-II(S) is quantized to a multiple of π due to the reflection symmetry while it has continuous values for UC-II(A). For both cases, the intercellular Zak phase shows the discrete jump at every Dirac node as in the 2D toy model-I.

We consider two terminated systems called Ribbon-II(A) and Ribbon-II(S), which are commensurate with UC-II(A)
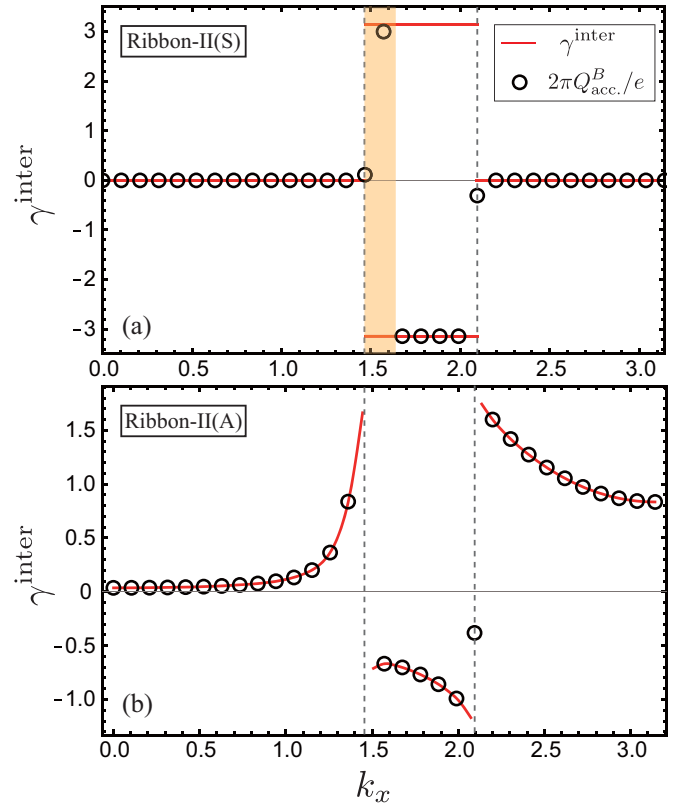

FIG. 8. Calculations of the intercellular Zak phases for (a) UC-II(S) and (b) UC-II(A). They are compared with the extra charge accumulations in the bottom surfaces of Ribbon-II(S) and Ribbon-II(A) which are marked by empty circles. The positions of the Dirac nodes are shown by vertical dashed lines. The shaded region in (a) is where the bulk-boundary correspondence fails because the Fermi level of the 1D effective Hamiltonian for given k_x is located at the edge of the bulk continuum as shown in Figs. 9(a) and 9(b).

and UC-II(S) each. As in the toy model-I, they are terminated along the x axis. We plot the extra charge accumulations in the bottom surface of those systems in Fig. 8. For the case of Ribbon-II(S), we break the reflection symmetry slightly so that one of the equivalent intercellular Zak phases π and $-\pi$ is selected to describe the extra charge accumulation in the bottom surface. One can note that the extra charge accumulation is well described by the intercellular Zak phase for all values of k_x except those in the shaded interval. This failure in this region is because the condition that the finite system is also insulating is violated. As shown in Fig. 9(b), in the shaded region, the topmost band at half-filling joins the conduction band continuum. Here, "half-filling" means the effective 1D system at each k_x is half-filled. Also, in this region, the states on the topmost band are no longer exponentially localized. On the other hand, in Ribbon-II(S), one can see the extra charge accumulation perfectly agrees with the intercellular Zak phase everywhere. This is because, in this case, the topmost band at half-filling belongs to the valence band continuum or is located in the middle of the bulk gap and shows a finite gap with empty upper levels as exhibited in Fig. 9(d). While the correspondence between the intercellular Zak phase and the extra charge accumulation is
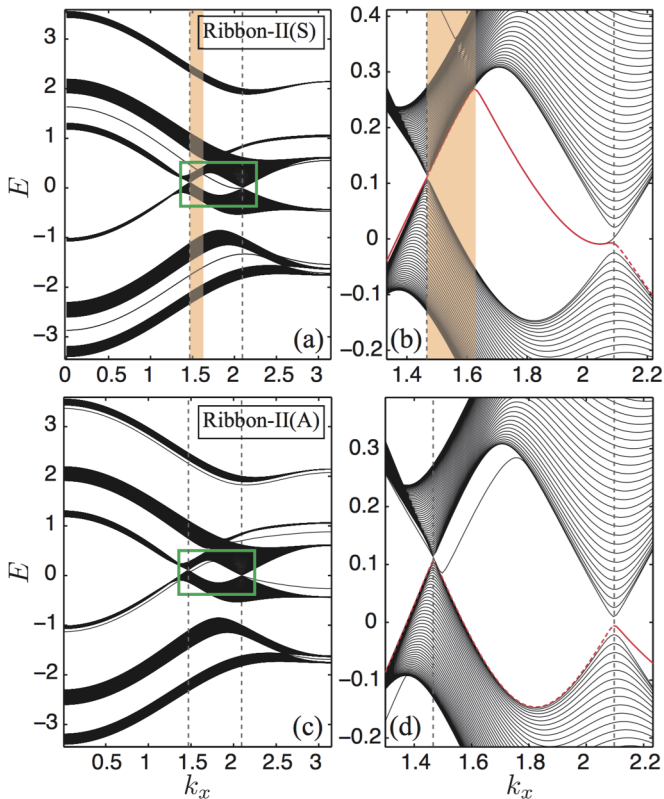
FIG. 9. Energy spectra of Ribbon-II(S) and Ribbon-II(A) are plotted in (a) and (c). A zoom into the region covered by the green boxes is given in (b) and (c). The meaning of the vertical dashed lines and the shaded regions is explained in Fig. 8. In (b) and (d), the red curves are the topmost filled band of the effective 1D system for given k_x at half-filling. If the wave function of this band is localized at the surface, we represent it by a solid curve. On the other hand, if the eigenstate is bulklike, it is drawn with a dashed line.

inaccurate only around the Dirac nodes where the system is metallic, one can reduce this inaccuracy to any desired value by increasing the surface region.

Finally, applying the modified bulk-boundary correspondence of Sec. IV, one can predict the number of surface bands in the gap (even or odd) in the inversion-symmetric case. From the intercellular Zak phase results in Fig. 8(a), one expects an even number of surface bands for $\gamma^{\text{inter}} = 0$ and an odd number of them for $\gamma^{\text{inter}} = \pi$ below the Fermi level of the effective 1D system at each k_x, except in the shaded region. As shown in Fig. 9(b), the number of surface modes below the Fermi level is two for $k_x < 1.468$ and zero for $k_x > 2.0944$, which correspond to the intervals where the intercellular Zak phase is zero. On the other hand, there is only one filled surface mode in $1.468 < k_x < 2.0944$, except in the shaded part.

VI. CONCLUSIONS

In this work, we have demonstrated that the intercellular Zak phase γ^{inter} can predict whether the number of surface modes below the Fermi level in 1D insulators is even or odd, when the commensurate bulk unit cell respects inversion symmetry. While the Zak phase itself cannot do this due to its arbitrariness depending on the choice of the real-space

origin and the unit cell, we have shown that γ^{inter}, as an origin-independent quantity, can be exploited for this bulk-boundary correspondence. Although γ^{inter} also depends on the unit-cell choice, it is not arbitrary once we select a unit cell that is commensurate with the finite system. Our bulk-boundary correspondence using γ^{inter} was justified with a microscopic interpretation of γ^{intra} and γ^{inter}. We explicitly showed that γ^{intra} is the electronic part of the bulk dipole moment of the unit cell, and γ^{inter} represents how much weight of the Wannier functions is exchanged with respect to a unit-cell boundary. When the system is terminated, γ^{intra} is interpreted as the classical bound surface charge, while γ^{inter} is understood as the extra charge accumulation around surfaces. Since the number of surface modes is closely related to the extra charge accumulation, we argue how it is related to γ^{inter} when the commensurate unit cell preserves inversion symmetry. If the origin is at the inversion center, γ^{inter} becomes identical to the Zak phase, and our bulk-boundary correspondence reduces to the conventional one. Thereby, our work also clarifies the conditions under which the conventional bulk-boundary correspondence using the Zak phase works.

We expect that the extra charge accumulation can be measured by scanning quantum dot microscopy (SQDM) [58]. SQDM offers three-dimensional images of electrostatic potentials down to the subnanometer level from which one could infer the total amount of its source charge. Since the electric field caused by extra charge accumulations at opposite edges of a long enough 1D chain can be considered independent, the extra charge accumulation at one edge can be obtained from the local electrostatic potential profile. Therefore, SQDM could be the characterizing experiment for the intercellular Zak phase like the capacitance measurement for the Zak phase.

APPENDIX A: INTRACELLULAR AND INTERCELLULAR ZAK PHASES

When we calculate the Zak phase, the momentum derivative operates on the exponential factor $e^{ik(ma-x)}$ and the coefficient $\alpha_k^{n,i,\zeta}$ of the lattice periodic part of the Bloch function (6). That is,

$$\gamma_n = i \int_{\text{BZ}} dk \langle u_{n,k} | \partial_k u_{n,k} \rangle \tag{A1}$$

$$= i \int_{\text{BZ}} dk \left\langle u_{n,k} \left| \sum_{m,i,\zeta} \alpha_k^{n,i,\zeta} \phi_m^{i,\zeta}(x)(\partial_k e^{ik(ma-x)}) \right\rangle \right.$$

$$+ i \int_{\text{BZ}} dk \left\langle u_{n,k} \left| \sum_{m,i,\zeta} (\partial_k \alpha_k^{n,i,\zeta}) \phi_m^{i,\zeta}(x) e^{ik(ma-x)} \right\rangle. \right. \tag{A2}$$

The first term is defined as the intracellular Zak phase and the second as the intercellular Zak phase.

First, the intracellular Zak phase is evaluated as follows:

$$\gamma_n^{\text{intra}} = i \int_{\text{BZ}} dk \int_\Omega dx \sum_{m,m'}^{N} \sum_{i,i'=1}^{N_b} \sum_{\zeta,\zeta'=1}^{N_{orb}^i} \alpha_k^{n,i,\zeta*} \phi_m^{i,\zeta}(x)^* e^{-ik(ma-x)} \alpha_k^{n,i',\zeta'} \phi_{m'}^{i',\zeta'}(x) \frac{\partial e^{ik(m'a-x)}}{\partial k} \tag{A3}$$

$$= \int_{\text{BZ}} dk \int_\Omega dx \sum_{m,m'}^{N} \sum_{i,i'=1}^{N_b} \sum_{\zeta,\zeta'=1}^{N_{orb}^i} (x-m'a) \alpha_k^{n,i,\zeta*} \alpha_k^{n,i',\zeta'} \phi_m^{i,\zeta}(x)^* \phi_{m'}^{i',\zeta'}(x) e^{ik(m'-m)a} \tag{A4}$$

$$= \int_{\text{BZ}} dk \int_\Omega dx \, x \sum_{m,m'}^{N} \sum_{i,i'=1}^{N_b} \sum_{\zeta,\zeta'=1}^{N_{orb}^i} \alpha_k^{n,i,\zeta*} \alpha_k^{n,i',\zeta'} \phi_m^{i,\zeta}(x)^* \phi_{m'}^{i',\zeta'}(x) e^{ik(m'-m)a} - m_\Omega a \int_{\text{BZ}} dk \sum_{i=1}^{N_b} \sum_{\zeta=1}^{N_{orb}^i} |\alpha_k^{n,i,\zeta}|^2 \tag{A5}$$

$$= N \int_{\text{BZ}} dk \int_\Omega dx \, x \left| \frac{1}{\sqrt{N}} \sum_m^N \sum_{i=1}^{N_b} \sum_{\zeta=1}^{N_{orb}^i} \alpha_k^{n,i,\zeta} \phi_m^{i,\zeta}(x) e^{ikma} \right|^2 - 2\pi m_\Omega \tag{A6}$$

$$= N \int_{\text{BZ}} dk \int_\Omega dx \, x |\psi_{n,k}(x)|^2 - 2\pi m_\Omega, \tag{A7}$$

where m_Ω is the index of the unit cell Ω. From (A4) to (A5), we used the orthonormality condition of the Löwdin functions $\int_\Omega dx \, \phi_m^{i,\zeta}(x)^* \phi_{m'}^{i',\zeta'}(x) = \delta_{m,m_\Omega} \delta_{m',m_\Omega} \delta_{i,i'} \delta_{\zeta,\zeta'}$. The second term of (A6) is obtained because the coefficients of the eigenstate for every n and k are normalized.

Second, the intercellular Zak phase is calculated as

$$\gamma_n^{\text{inter}} = i \int_{\text{BZ}} dk \int_\Omega dx \sum_{m,m'}^{N} \sum_{i,i'=1}^{N_b} \sum_{\zeta,\zeta'=1}^{N_{orb}^i} \alpha_k^{n,i,\zeta*} \phi_m^{i,\zeta}(x)^* e^{-ik(ma-x)} \frac{\partial \alpha_k^{n,i',\zeta'}}{\partial k} \phi_{m'}^{i',\zeta'}(x) e^{ik(m'a-x)} \tag{A8}$$

$$= i \int_{\text{BZ}} dk \sum_{m,m'}^{N} \sum_{i,i'=1}^{N_b} \sum_{\zeta,\zeta'=1}^{N_{orb}^i} \alpha_k^{n,i,\zeta*} e^{-ikma} \frac{\partial \alpha_k^{n,i',\zeta'}}{\partial k} e^{ikm'a} \delta_{m,m_\Omega} \delta_{m',m_\Omega} \delta_{i,i'} \delta_{\zeta,\zeta'} \tag{A9}$$

$$= i \sum_{i=1}^{N_b} \sum_{\zeta=1}^{N_{orb}^i} \int_{\text{BZ}} dk \, \alpha_k^{n,i,\zeta*} \frac{\partial}{\partial k} \alpha_k^{n,i,\zeta}. \tag{A10}$$

The intercellular Zak phase is represented by the Wannier coefficients $A_m^{n,i,\zeta}$ by using the inverse transformation of (16), which is given by

$$\alpha_k^{n,i,\zeta} = \sum_m^N A_m^{n,i,\zeta} e^{-ikma}. \tag{A11}$$

Substituting into Eq. (A10), we have

$$\gamma_n^{\text{inter}} = \sum_{i,\zeta} \sum_{m,m'} \int_{\text{BZ}} dk \, m \, A_m^{n,i,\zeta*} A_{m'}^{n,i,\zeta} e^{ik(m-m')a} \tag{A12}$$

$$= 2\pi \sum_m \sum_i^{N_b} \sum_\zeta^{N_{orb}^i} m |A_m^{n,i,\zeta}|^2, \tag{A13}$$

where the summation ranges of i and ζ are the same as those of (A10).

We further split γ_n^{inter} into $\gamma_n^{R\to L}$ and $\gamma_n^{R\to L}$, which satisfies $\gamma_n^{\text{inter}} = -\gamma_n^{R\to L} + \gamma_n^{R\to L}$, as follows:

$$\gamma_n^{R\to L} = -2\pi \sum_{m=-\infty}^{-1} \sum_{i=1}^{N_b} \sum_{\zeta=1}^{N_{orb}^i} m |A_m^{n,i,\zeta}|^2 \tag{A14}$$

$$= 2\pi \sum_{m'=0}^{\infty} \sum_{m=-\infty}^{-1} \sum_{i=1}^{N_b} \sum_{\zeta=1}^{N_{orb}^i} |A_{m-m'}^{n,i,\zeta}|^2 \tag{A15}$$

$$= 2\pi \sum_{m'=0}^{\infty} \int_{-\infty}^{x_b} dx |W_{n,m'}(x)|^2 \tag{A16}$$

and

$$\gamma_n^{L\to R} = 2\pi \sum_{m=0}^{\infty} \sum_{i=1}^{N_b} \sum_{\zeta=1}^{N_{orb}^i} m |A_m^{n,i,\zeta}|^2 \tag{A17}$$

$$= 2\pi \sum_{m'=-\infty}^{-1} \sum_{m=0}^{\infty} \sum_{i=1}^{N_b} \sum_{\zeta=1}^{N_{orb}^i} |A_{m-m'}^{n,i,\zeta}|^2 \tag{A18}$$

$$= 2\pi \sum_{m'=-\infty}^{-1} \int_{x_b}^{\infty} dx |W_{n,m'}(x)|^2, \tag{A19}$$

where x_b is the boundary between the $m = -1$ and the 0 unit cells. Although we specify the boundary x_b, the result is independent of it due to translational invariance, as it is clear from the dependence on $m - m'$ in Eqs. (A15) and (A18).

APPENDIX B: BOUND SURFACE CHARGE

In this section, we show that the bound surface charge can be split into the classical bound surface charge and the extra charge accumulation. The bound surface charge of the left edge is given by

$$\sigma^{LS} = \frac{1}{a} \int_{-\infty}^{x_c} dx \int_{x-\frac{a}{2}}^{x+\frac{a}{2}} dx' \rho_{\text{t.s.}}(x') = \int_{-\infty}^{x_c} dx \, \bar{\rho}_{\text{t.s.}}(x), \quad \text{(B1)}$$

where $\rho_{\text{t.s.}}(x)$ is the total charge density including both the electronic and ionic contributions $\bar{\rho}_{\text{t.s.}}(x) = a^{-1} \int_{x-\frac{a}{2}}^{x+\frac{a}{2}} dx' \rho_{\text{t.s.}}(x')$, and x_c is an arbitrary position in the finite system, far away from the surfaces compared with the widths of the φ_l^{LS}'s.

First, note that σ^{LS} is independent of x_c since

$$\frac{\partial \sigma^{LS}}{\partial x_c} = \frac{1}{a} \int_{x_c - \frac{a}{2}}^{x_c + \frac{a}{2}} dx' \rho_{\text{t.s.}}(x) = \bar{\rho}_{\text{t.s.}}(x_c) \quad \text{(B2)}$$

vanishes when x_c is far from the surfaces. The integral of the charge density over one unit-cell length a is zero far from the surfaces because our system is assumed to be neutral.

Second, the expression for the bound surface charge can transformed as follows:

$$\sigma^{LS} = - \int_{-\infty}^{x_c} dx \frac{d\bar{\rho}_{\text{t.s.}}(x)}{dx} x + \bar{\rho}_{\text{t.s.}}(x)x \Big|_{-\infty}^{x_c} \quad \text{(B3)}$$

$$= -\frac{1}{a} \int_{-\infty}^{x_c} dx \left[\rho_{\text{t.s.}}\left(x + \frac{a}{2}\right) - \rho_{\text{t.s.}}\left(x - \frac{a}{2}\right) \right] x \quad \text{(B4)}$$

$$= -\frac{1}{a} \int_{x_c - \frac{a}{2}}^{x_c + \frac{a}{2}} dx \, \rho_{\text{t.s.}}(x)x + \int_0^{x_c - \frac{a}{2}} dx \, \rho_{\text{t.s.}}(x), \quad \text{(B5)}$$

where $x_{\pm} = x \pm a/2$. We have used the fact that $\bar{\rho}_{\text{t.s.}}(x_c) = \bar{\rho}_{\text{t.s.}}(-\infty) = 0$ in going from (B3) to (B4), and that $\rho_{\text{t.s.}}(x) = 0$ for $x < 0$ from (B4) to (B5). If $x_c = x_{\ell_L} + a/2$, we have

$$\sigma^{LS} = -\frac{1}{a} \int_{x_{\ell_L}}^{x_{\ell_L} + a} dx \, x\rho_{\text{t.s.}}(x) + \int_0^{x_{\ell_L}} dx \, \rho_{\text{t.s.}}(x). \quad \text{(B6)}$$

In the same way, the bound surface charge at the right edge becomes

$$\sigma^{RS} = \frac{1}{a} \int_{x_{N-\ell_R} - a}^{x_{N-\ell_R}} dx \, x\rho_{\text{t.s.}}(x) + \int_{x_{N-\ell_R}}^{x_N} dx \, \rho_{\text{t.s.}}(x). \quad \text{(B7)}$$

These are the expressions for the bound surface charges used in (38) and (39) in Sec. III.

[1] M. V. Berry, Proc. R. Soc. Lond. A **392**, 45 (1984).
[2] J. Zak, Phys. Rev. Lett. **62**, 2747 (1989).
[3] R. D. King-Smith and D. Vanderbilt, Phys. Rev. B **47**, 1651 (1993).
[4] D. Vanderbilt and R. D. King-Smith, Phys. Rev. B **48**, 4442 (1993).
[5] R. Resta, Rev. Mod. Phys. **66**, 899 (1994).
[6] N. A. Spaldin, J. Solid State Chem. **195**, 2 (2012).
[7] C. L. Kane and E. J. Mele, Phys. Rev. Lett. **95**, 146802 (2005).
[8] C. L. Kane and E. J. Mele, Phys. Rev. Lett. **95**, 226801 (2005).
[9] B. A. Bernevig, T. L. Hughes, and S.-C. Zhang, Science **314**, 1757 (2006).
[10] L. Fu, C. L. Kane, and E. J. Mele, Phys. Rev. Lett. **98**, 106803 (2007).
[11] L. Fu and C. L. Kane, Phys. Rev. B **76**, 045302 (2007).
[12] M. Z. Hasan and C. L. Kane, Rev. Mod. Phys. **82**, 3045 (2010).
[13] X.-L. Qi and S.-C. Zhang, Rev. Mod. Phys. **83**, 1057 (2011).
[14] L. Fu, Phys. Rev. Lett. **106**, 106802 (2011).
[15] S. Matsuura, P.-Y. Chang, A. P. Schnyder, and S. Ryu, New J. Phys. **15**, 065001 (2013).
[16] Y. Hatsugai, J. Phys. Soc. Jpn. **75**, 123601 (2006).
[17] S. Ryu and Y. Hatsugai, Phys. Rev. B **73**, 245115 (2006).
[18] P. Delplace, D. Ullmo, and G. Montambaux, Phys. Rev. B **84**, 195452 (2011).
[19] T. Kariyado and Y. Hatsugai, Phys. Rev. B **88**, 245126 (2013).
[20] F. Grusdt, M. Höning, and M. Fleischhauer, Phys. Rev. Lett. **110**, 260405 (2013).
[21] R. Barnett, Phys. Rev. A **88**, 063631 (2013).
[22] Y.-H. Chan, C.-K. Chiu, M. Y. Chou, and A. P. Schnyder, Phys. Rev. B **93**, 205132 (2016).
[23] A. A. Soluyanov and D. Vanderbilt, Phys. Rev. B **83**, 035108 (2011).
[24] W. B. Hodge, E. D. Welchman, and M. J. Rave, Eur. Phys. J. B **84**, 351 (2011).
[25] M. Atala, M. Aidelsburger, J. T. Barreiro, D. Abanin, T. Kitagawa, E. Demler, and I. Bloch, Nat. Phys. **9**, 795 (2013).
[26] S. Longhi, Opt. Lett. **38**, 3716 (2013).
[27] J. C. Budich and E. Ardonne, Phys. Rev. B **88**, 035139 (2013).
[28] Y. Yoshimura, K.-I. Imura, T. Fukui, and Y. Hatsugai, Phys. Rev. B **90**, 155443 (2014).
[29] A. Alexandradinata, C. Fang, M. J. Gilbert, and B. A. Bernevig, Phys. Rev. Lett. **113**, 116403 (2014).
[30] F. de Juan, A. Rüegg, and D.-H. Lee, Phys. Rev. B **89**, 161117(R) (2014).
[31] C. W. Ling, M. Xiao, C. T. Chan, S. F. Yu, and K. H. Fung, Opt. Express **23**, 2021 (2015).
[32] A. Przysiężna, O. Dutta, and J. Zakrzewski, New J. Phys. **17**, 013018 (2015).
[33] W.-R. Lee and K. Park, Phys. Rev. B **92**, 195144 (2015).
[34] Y.-X. Xiao, Z.-Q. Zhang, and C. T. Chan, arXiv:1605.00549.
[35] L. Fidkowski, T. S. Jackson, and I. Klich, Phys. Rev. Lett. **107**, 036601 (2011).
[36] A. Alexandradinata, X. Dai, and B. A. Bernevig, Phys. Rev. B **89**, 155114 (2014).
[37] M. Taherinejad, K. F. Garrity, and D. Vanderbilt, Phys. Rev. B **89**, 115102 (2014).
[38] Z. Wang, A. Alexandradinata, R. J. Cava, and B. A. Bernevig, Nature (London) **532**, 189 (2016).
[39] A. Alexandradinata, Z. Wang, and B. A. Bernevig, Phys. Rev. X **6**, 021008 (2016).
[40] A. Alexandradinata and B. A. Bernevig, Phys. Rev. B **93**, 205104 (2016).
[41] C. Fang, Y. Chen, H.-Y. Kee, and L. Fu, Phys. Rev. B **92**, 081201(R) (2015).

[42] M. Hirayama, R. Okugawa, T. Miyake, and S. Murakami, arXiv:1602.06501.

[43] K. N. Kudin, R. Car, and R. Resta, J. Chem. Phys. **126**, 234101 (2007).

[44] If there are non-negligible overlaps between atomic orbitals at different sites, we can choose $\{\phi_m^{i,\zeta}(x)\}$ to be the Löwdin functions [59,60] which satisfy the orthonormal condition even for those at different sites while preserving the point-group symmetries of the original atomic wave functions.

[45] W. Kohn, Phys. Rev. **115**, 809 (1959).

[46] G. Nenciu, Commun. Math. Phys. **91**, 81 (1983).

[47] G. Panati, Ann. Henri Poincarè **8**, 995 (2007).

[48] M. Kohmoto, Ann. Phys. (NY) **160**, 343 (1985).

[49] C. Brouder, G. Panati, M. Calandra, C. Mourougane, and N. Marzari, Phys. Rev. Lett. **98**, 046402 (2007).

[50] W. Kohn and J. R. Onffroy, Phys. Rev. B **8**, 2485 (1973).

[51] J. J. Rehr and W. Kohn, Phys. Rev. B **10**, 448 (1974).

[52] C. Kallin and B. I. Halperin, Phys. Rev. B **29**, 2175 (1984).

[53] A. Baldereschi, S. Baroni, and R. Resta, Phys. Rev. Lett. **61**, 734 (1988).

[54] K. N. Kudin, R. Car, and R. Resta, J. Chem. Phys. **127**, 194902 (2007).

[55] J.-H. Park, G. Yang, J. Klinovaja, P. Stano, and D. Loss, Phys. Rev. B **94**, 075416 (2016).

[56] M. J. Rice and E. J. Mele, Phys. Rev. Lett. **49**, 1455 (1982).

[57] W. P. Su, J. R. Schrieffer, and A. J. Heeger, Phys. Rev. Lett. **42**, 1698 (1979).

[58] C. Wagner, M. F. B. Green, P. Leinen, T. Deilmann, P. Krüger, M. Rohlfing, R. Temirov, and F. S. Tautz, Phys. Rev. Lett. **115**, 026101 (2015).

[59] P. Löwdin, J. Chem. Phys. **18**, 365 (1950).

[60] J. C. Slater and G. F. Koster, Phys. Rev. **94**, 1498 (1954).